Motion of a Rotor in Retainer Bearings

M. Fumagalli, G. Schweitzer

Internat. Center for Magnetic Bearings
ETH Zurich, 8092 Zurich, Switzerland
fax: +41-1-632 10 78; e-mail: cassoli@ifr.mavt.ethz.ch; http://www.ifr.mavt.ethz.ch

Abstract

The experimental results on the contact interaction of a spinning rotor with its retainer bearing, and the onset of the whirl motion are shown together with an analysis. Measurement data for various material combinations and for ball bearings are presented.

1 Introduction

During contact between a high speed rotor and a stationary body, the high energy of the rotor, which is then dissipated by frictional forces, can severely damage both parts. This contact interaction can occur in high speed rotors, supported by active magnetic bearings (AMB), when the magnetic bearing fails. The understanding of the dynamics of a rotor in retainer bearings, i.e: the forces, energy losses and the effect of parameters such as the coefficient of friction on the motion, is imperative to assure the reliable function of the retainer bearing. Retainer bearings are a central safety component of an AMB.

For some time various studies have been performed on the dynamics of high speed rotors in retainer bearings [1 to 5]. Feeny [6] developed the equations of motion for a perfectly balanced rotor in contact with retainer bearings for nearly conical and cylindrical motion, and a local analysis of these configurations was performed.

The rotor dynamics literature on rotor/stator contact interaction shows a wealth of models and rotor behaviours. The Brite/Euram project "Rostadyn" on rotor-stator interaction dynamics aims to provide European manufacturers of rotating machinery with design methods to build vibration resistant machines of the highest efficiency [7]. More extensive literature is given, for example, by Muszynska [8] or in the recent thesis of Isaksson [9]. There are numerous results on contact dynamics, however, an understanding of forces and energy dissipation during different phases of the motion is still desirable.

In this paper, the experimental results on the onset of whirl motion will be shown together with an analysis of the measured data on motion, velocities, forces and power losses during cylindrical motion. The experiments consist of shutting down the bearings of a magnetically suspended rotor simultaneously, letting the rotor fall down into a specially instrumented contact bearing, and initiating a whirl motion. Stators made of carbon graphite, beryllium bronze, nylon, an elastically suspended bronze ring and a ball bearing have been tested.

The measurements of the interaction between a rotor and its stator show that during whirl motion, the whirl velocity increases until it locks to the first elastic eigenfrequency of the rotor, rigidly supported at both ends, and usually it increases from then on depending on the energy transferred to the whirl motion by the sliding rotor.

2 Planar Rotor Motion

2.1 Mechanical Model

To begin with, we designed a planar model on the assumption that a cylindrical motion exists and is stable [6]. Figure 1 shows the coordinate system of the mechanical model. Rotation refers to the clockwise spinning motion about the axis of the shaft, and is labeled ϕ. The spin velocity is $\dot{\phi}$. Revolution refers to the motion within the ring, and is labeled θ, its derivative is $\dot{\theta}$. The revolution motion around the bearing is also called whirl motion. The perfectly balanced, rigid rotor has mass m, rotational inertia J, and radius r. The rigidly supported bearing has radius R. The air

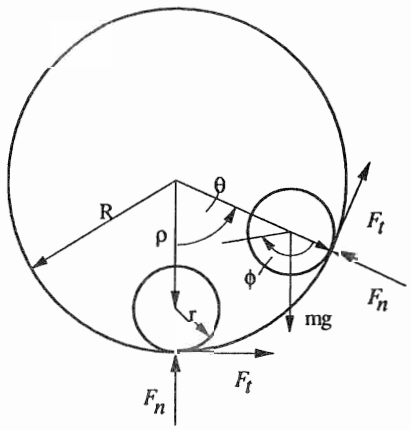

Fig. 1 Mechanical model

gap ρ is the difference between the bearing radius and rotor radius $\rho = (R\text{-}r)$. The sliding motion of the rotor is governed by Coulomb friction μ; the gravitational acceleration g is taken into account.

2.2 Sliding and Rolling Motion

The equations of motion, given in [1], are summarized briefly. Sliding occurs when there is a relative velocity at the contact point between the rotor and the bearing surface. If the rotor is rolling, the contact point has no velocity, and it is the instantaneous centre of rotation. These kinematics lead to the rolling condition

$$\dot{\theta} = \dot{\phi} r / \rho \tag{1}$$

In general, the air gap is very small and the spin velocity is very high. If the rotor enters a revolutional motion and is constrained to roll, theory leads to practically unrealistically high values for the whirl velocity $\dot{\theta}$. Equations of motion for the spin and the whirl motion are given by

$$m\rho\ddot{\theta} + mg\sin\theta - \mu m(g\cos\theta + \rho\dot{\theta}^2)\,sign(\dot{\phi}r - \dot{\theta}\rho) = 0$$

$$J\ddot{\phi} + \mu m r(g\cos\theta + \rho\dot{\theta}^2)\,sign(\dot{\phi}r - \dot{\theta}\rho) = 0 \tag{2}$$

The equations are valid when $\dot{\phi}r \neq \dot{\theta}\rho$ and the normal load is nonnegative,so that

$$g\cos\theta + \rho\dot{\theta}^2 \geq 0 \tag{3}$$

The equation for the whirl describes the motion of a pendulum that is self excited by frictional force. It was already pointed out, that in our magnetic bearing application the spin velocity is rather high, thus the $sign(\dot{\phi}r - \theta\rho)$ can be considered positive, i.e the direction of the frictional force is practically independent of the magnitude of the relative sliding velocity at the contact point. In such a case of pure sliding, the magnitude of the rotation has no direct effect on the whirl of the rotor. The physical effects, however, that are to be expected at high relative velocities (above, for example, 300 m/s), are probably not considered in Coulomb's law. They are unknown and should be investigated and modelled in future research.

2.3 Force and Energy Loss

The forces in the cylindrical motion represent the "worst case" if the rotor whirls around the entire bearing. Then the centripetal effects are predominant. During a purely cylindrical motion, $\dot{\theta}$ increases while $\dot{\phi}$ decreases until the onset of whirl. Neglecting the gravitational force, the spin deceleration is approximated by

$$\ddot{\phi} \cong -\mu m\rho\dot{\theta}^2 r / J \tag{4}$$

and the acceleration of the whirl motion is given by

$$\ddot{\theta} \cong \mu\dot{\theta}^2 \tag{5}$$

The normal force on each bearing during the cylindrical motion is given by

$$F_{cyl} = m\rho\dot{\theta}^2 / 2 \tag{6}$$

The total kinetic energy for the cylindrical motion is

$$E_{cyl} = E_{spin} + E_{whirl} = J\dot{\phi}^2 / 2 + m\rho^2\dot{\theta}^2 / 2 \tag{7}$$

and the power dissipation due to the deceleration of the spin motion follows from differentiating E_{spin} with respect to time and substituting for $\ddot{\phi}$ in equation (4)

$$P_{spin} = -\mu m\rho\dot{\theta}^2\dot{\phi}r \tag{8}$$

The power loss, arising between a rotor and stator during interaction, can reach rather high values. It can produce very high temperatures at the contact surfaces. Depending upon the material, the stator or the rotor will retain the largest part of thermal energy, which may cause deformation or damage to that part. The power loss calculation is therefore very important to find an adequate design and to verify the model.

3 Test Rig

A test rig has been built at the ETH with the main objective measuring contact dynamics, primarily the first contact and the onset of the contact induced vibrations. Figure 2 shows the general procedure, details on the test rig are given in [10]. The rotor is suspended in contact free magnetic bearings. By suitably actuating these magnetic bearings, any initial condition for a contact at a specially instrumented, elastically suspended touch down ring can be generated. The ring can be made of different materials such as bronze, steel, nylon, or ceramic. The test rig has the main specifications

Max. speed of the rotor	$\dot{\phi}$	=	30 000 r/min
Mass	m	=	3.36 kg
Length	L	=	326 mm
Touch down ring radius	r	=	10 mm
Air gap	ρ	=	0.3 mm
Polar moment of inertia	J	=	6.72 10^{-4} kg m^2
Material of rotor surface			steel

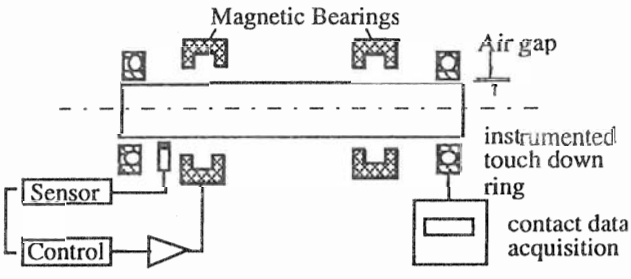

Fig 2 Test rig for measuring contact dynamics

4 Measurements on Whirl Motions

The experiment was started by shutting down both magnetic bearings and the motor drive, while the rotor speed was 24 000 r/min. The initial position of the rotor was off center in such a way, that, after a free fall phase, the impact velocity had a sufficiently large component tangential to the housing and in the direction of the reverse whirl. Figure 3 pictures a pre whirling stage between 0.2 and 0.3 s, which finally turns into a whirling motion. At 0.23 s the rotor makes permanent contact with the stator. After the first revolution, the whirling velocity of the rotor is $\dot{\theta} = 95$ Hz. This is a sufficiently large initial condition for the rotor to start a permanent whirl. After five revolutions, the rotor accelerates in about 0.03 s to the final whirl velocity $\dot{\theta} = 190$ Hz. This phenomenon of a limiting whirl velocity will be discussed in connection with figure 5.

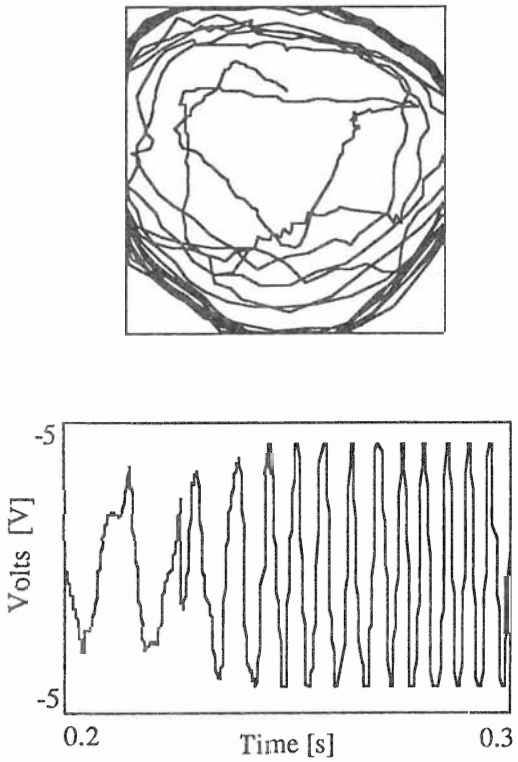

Fig 3 Pre whirl motion, trajectory of the rotor and time history of the displacement in a lateral direction

Figure 4 shows the end of the whirl motion of fig. 3. The spin velocity is rapidly decreasing and the spin motion stops abruptly at about 0.75 s while the whirl still continues for some time. Only shortly before the run down of the rotor, at about 0.6 s, is the kinematic rolling condition achieved during phase 3 of the motion, which will be explained in 5.1.

Measurements of the contact forces during the initial contact and a mechanical model for the vibroimpact are described in [11].

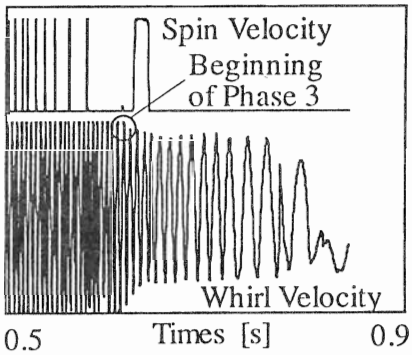

Fig 4 Spin velocity, indicated by a pulse for each rotor turn, and displacements of the rotor in lateral direction, illustrating the whirl motion from 0.5 sec on and, in particular, the final run down

5 Analysis of Whirl Measurements

In this section the results of the measurements analysis will be shown. Measurements are analysed with respect to the rotor's motion, its velocity, the acting forces and power loss. Results will be presented that refer to the whirl itself without the initial phase, using different materials for the retainer bearing

5.1 Stator made of a Graphite Ring

Both magnetic bearings and motor drive were shut down, at a rotor speed of 21 000 r/min. The time behaviour of various variables is shown in figure 5. To explain the measurements for the whirl motion, they can be considered to be divided into three phases which are indicated in the figure.

Phase 1 can be desribed by the equations of motion (2) for the planar model. It begins when the rotor makes permanent contact with the stator and ends when the whirl frequency reaches the first elastic eigenfrequency $\dot{\theta}_{r1}$ of the rotor, rigidly supported at the contact areas at both ends. This phenomenon is not included in our simple rigid rotor model; its existence, however, has been predicted by Black [12] and experimentally shown by Lingener [13]. The calculated eigenfrequency $\dot{\theta}_{r1}$ was about 300 Hz and the measured one 270 Hz. The spin velocity $\dot{\phi}$ is reduced by frictional forces from initially 350 Hz to 320 Hz, the coefficient of friction μ=0.14 follows from equation (4) together with the measurements on the kinematics. The spin energy E_{spin} has reduced to 1.4 kJ by the end of phase 1 and during this run down the power loss P_{spin} achieves a maximum value of 8 kW. The normal force F_{cyl} can be estimated from equation (6) to achieve a maximal value of about 0.9 kN. The energy transferred into the whirl motion is very small, $E_{whirl} = 0.2$ J, but quite sufficient to overcome the potential energy for lifting the rotor to its highest position within the small air gap.

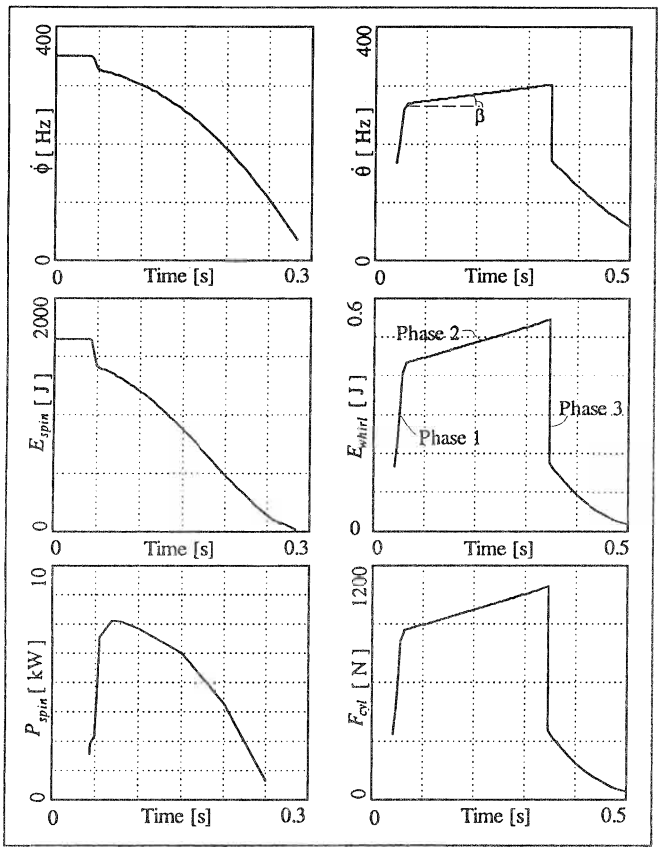

Fig. 5 Time history of the whirling motion when the steel rotor contacts a graphite retainer bearing for the variables spin velocity $\dot{\phi}$, whirl velocity $\dot{\theta}$, spin energy E_{spin}, whirl energy E_{whirl}, power loss of the spinning rotor P_{spin}, and normal force F_{cyl}

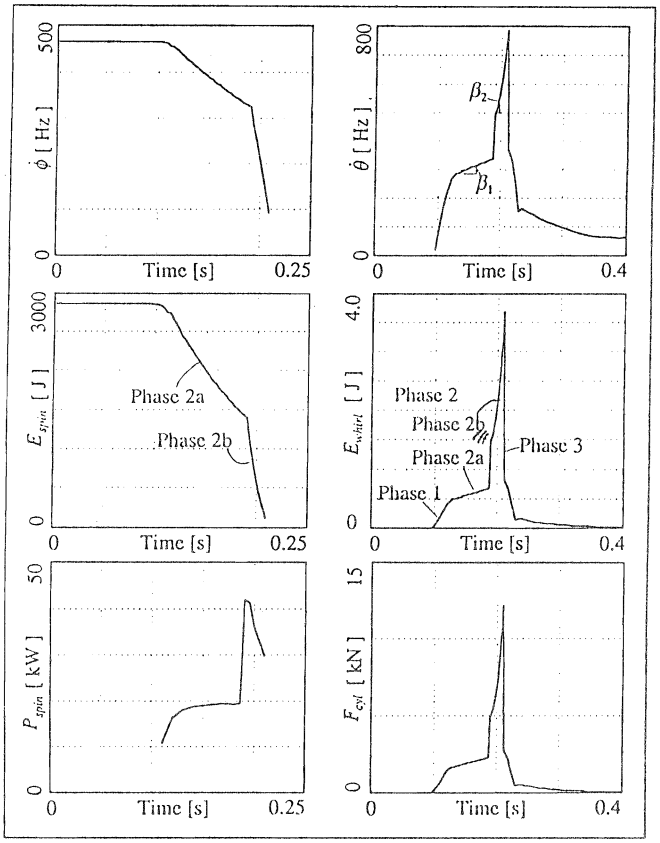

Fig. 6 Time history of contact variables as in fig. 5, for a retainer bearing made of Beryllium Bronze

Phase 2 represents the whirl motion itself. During this phase, the whirl velocity tends to the eigenfrequency $\dot{\theta}_{r1}$, it increases only slightly and linearly, depending on the energy dissipated by the vibrating stator and at the contact. It is well known that a similar "locking" phenomenon can occur when an elastic rotor passes a critical bending speed. It is a balance of energy which, on one hand, is supplied by the rotor through the frictional mechanism and which, on the other hand, is used to maintain and further build up the whirl.

Phase 3 begins when the rotor reaches the kinematic rolling condition (1). At this point the whirl velocity is $\dot{\theta}_{r1} \cong 300$ Hz, and the spin velocity 9 Hz. The subsequent, dramatic break down of the motion is also clearly seen in figure 4. The total time for the rotor to come to a complete standstill is less than 0.9 s. The experiments should not be carried out without some caution.

5.2 Stator made of Beryllium Bronze

The same test was performed, starting from a rotor speed of 28 000 r/min, with a retainer bearing made of beryllium bronze. Figure 6 shows that the whirl starts after 0.1 s, and again we can distinguish three separate phases of motion. In the first phase, the rotor accelerates up to the first elastic rigid-rigid frequency of $\dot{\theta}_{r1} = 280$ Hz. This frequency is somewhat higher than that obtained using carbon graphite. It reflects the fact that beryllium bronze is stiffer than the graphite material.

In the second phase an interesting wear phenomena occurs. The spin velocity shows two phases of decay, one in the interval from 0.1 s to 0.18 s, the other from 0.18 s to 0.2 s. For t > 0.18 s, wear between the rotor and the beryllium bronze must have occured along with an increase in friction. Due to this wear there is a higher energy transfer to the whirl motion, and consequently the whirl velocity increases drastically. Traces of wear could be observed on the beryllium bronze after disassembly. The micromechanics of that wear are not yet understood. The whirl velocity now achieves a peak value of $\dot{\theta} = 800$ Hz, resulting in a normal force of $F_{cyl} = 12$ kN. The spin velocity reaches zero in only 0.1 s. Due to wear between the materials, the power loss achieves a peak value of $P_{spin} = 45$ kW in the second phase.

The phase 3 begins when the rotor reaches a whirl velocity of $\dot{\theta} = 800$ Hz, and the spin velocity is down to $\dot{\phi} = 24$ Hz.

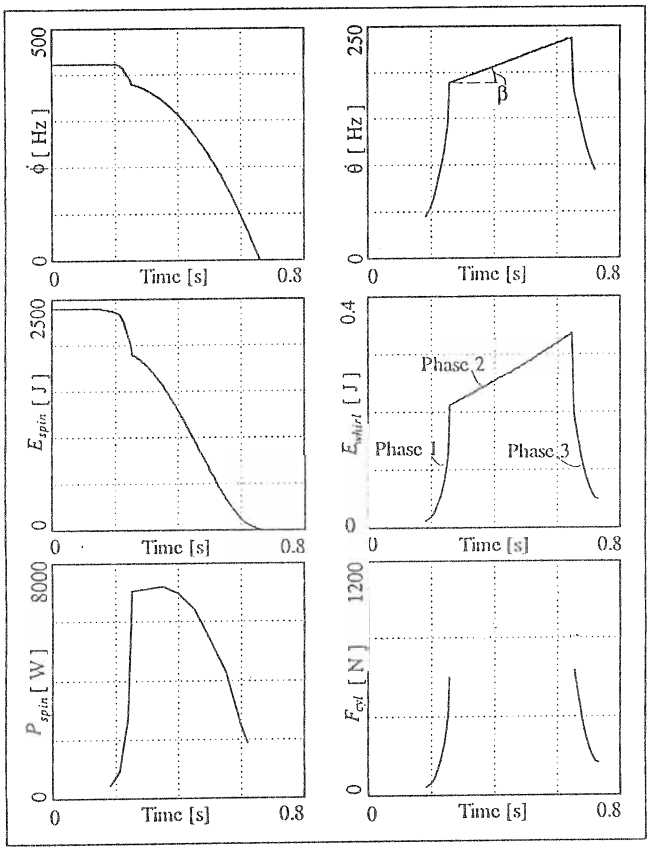

Fig 7 Time history of contact variables as in fig. 5, for a stator made of an elastically suspended Bronze ring

5.3 Stator made of an elastically suspended Bronze ring

Positioned at one side of the assembly was a rigid bronze ring and at the other side an elastically suspended bronze ring. The shut down was initiated with the rotor spinning at 24 000 rpm. Fig. 7 shows that after about 0.2 s the rotor makes permanent contact with the stator and the rotor accelerates to a coupled frequency of $\dot{\theta}_{rl} = 190$ Hz. This coupled eigenfrequency can be explained by the coupling between the rotor and stator eigenfrequencies. During phase one, the normal force reaches a value of $F_{cyl} = 650$ N, and the power loss an estimated maximum of $P_{spin} = 7.0$ kW.

During the second phase, the whirl motion increases only slightly until 240 Hz. This "locking" to the coupled eigenfrequency has some potential to be used for the design of a support for the retainer bearing. In this case the locking of the whirl would be reliably predictable and the locking at a low eigenfrequency would prevent higher whirl speeds and higher loads on the rotor. However, the soft suspension results in an undesirable large deformation of the rotor/bearing system which might cause the rotor to touch other parts of the assembly. The contact forces during that phase have not yet been measured, and they cannot be derived from equ. (6) as the rotor displacement may be different from the airgap ρ depending on the elastic suspension.

6 Touch Down in a Ball Bearing

The most common retainer bearings are ball bearings. The bearings, after a touch down, are accelerated in a very short time up to the rotor velocity [2]. During this high acceleration of the balls and the inner race, the high frictional forces can generate local hot spots and damage the bearings. After the acceleration phase, the relative velocity between the parts is virtually zero, and there is no longer any considerable energy transfer within the system.

The aim of the ball bearing measurements is to identify the sliding/rolling between the parts and to give some preliminary information on how to model the complex ball bearing motion.

In order to quantify the behaviour, two optical sensors measure the revolution of the ball cage and the inner ring. The tested bearing was a commercially available single row deep groove ball bearing (SKF 6004). It is a grease bearing with an outer diameter of 42 mm, an inner diameter of 20 mm, and it has a nominal limit speed of 12 000 r/min.

The rotor was dropped from a speed of 16 000 r/min. No whirl was excited, the rotor always stayed near or at the bottom of the bearing. In order to quantify the amount of sliding and rolling, the revolution of the balls together with the cage and the revolution of the inner race are shown in

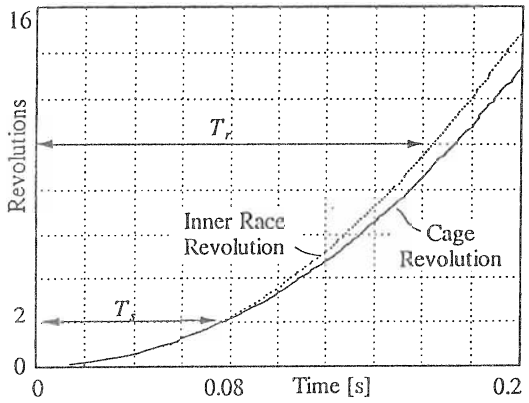

Fig. 8 Revolutions of the inner race and the cage after a touch down with a speed of 16 000 r/min

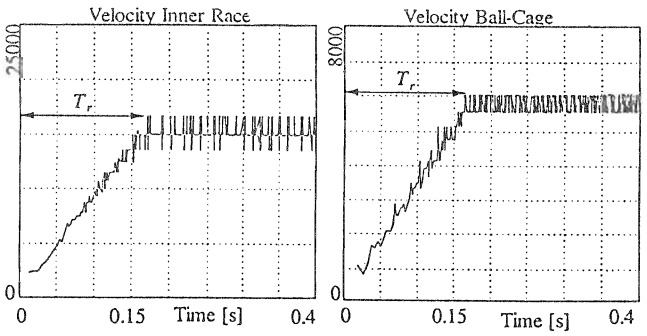

Fig. 9 Velocities of the inner race and the ball cage

fig. 8. Relating the revolution of the cage to that of the inner race we obtain a factor f, and if this factor is constant during most of the time, there is rolling motion between the parts. The motion in fig. 8 can be split into two phases. Firstly, for $t<T_S$, the frictional force accelerates the inner race almost synchronously with the cage up to a time T_S. During this time, the inner race and the ball cage rotate through approximately two revolutions each. Because the factor f is not constant during this time interval we can conclude that there is sliding between the inner race and the balls, and, of course, between the rotor and the inner race. After time T_S, a rolling motion between the bearing's parts takes place, and they are accelerated very quickly until they reach rotor velocity at time $T_r \cong 0.16$ s.

Figure 9 shows the velocities of the cage and the inner race, where the time T_r can be recognized more clearly. The time T_r can be defined as the time for all the parts to achieve rolling. Before that time there exists a sliding motion between the rotor and the inner race and a transfer of energy from the rotor to the bearing.

7 Conclusions

From the results, the following conclusions can be drawn.

The whirl velocity increases until it locks to the first elastic eigenfrequency of the rotor which is rigidly supported at both ends. The whirl velocity, from then on, increases only slightly due to the energy transfer to the whirl motion, and this energy appears to be an empirical value, related to friction. If such a low transfer energy to the whirl motion is to be expected (Steel/Graphite), the whirl velocity is known and the centrifugal force can be estimated.

However, if the energy transfer to the whirl motion is high (Steel/Bronze), the whirl velocity can increase drastically. In this case it is still difficult to estimate the maximum centrifugal forces.

If the retainer bearing is supported by an elastically suspended stator, the coupled eigenfrequency is smaller than the first elastic rigid-rigid eigenfrequency. The whirl locks to that coupled eigenfrequency, and the whirl velocity remains small. Consequently the resulting centrifugal forces remain equally small. However, the soft suspension results in an undesirable large deformation amplitude of the rotor/bearing system. There must, therefore, be a design compromise between force and deformation. The latter must be small enough to ensure that the rotor doesn't touch other parts of the assembly.

Acceleration of a ball bearing during touch down has been measured. The frictional forces, driving that acceleration, can be estimated, as well as the energy transfer between rotor and bearing. Results should be useful for deriving design rules for reliable and low cost retainer bearings.

8 References

[1] Fumagalli, M. A., Feeny, B., Schweitzer, G.; Dynamics of Rigid Retainer Bearings, *Third Internat. Symp. on Magnetic Bearings*, Washington, July 1992, pp. 157-166

[2] Dell, H., Engel, J., Faber, R., Glass, D.; Developments and Tests on Retainer Bearings for a Large Active Magnetic Bearing, *First Internat. Symp. on Magnetic Bearings*, Zurich, Springer-Verlag,1988

[3] Ishi, T., Kirk, G.R.; Transient Response Technique Applied to Active Magnetic Bearing Machinery During Rotor Drop, *13th Bienl. Conf. on Mech. Vibration and Noise*, ASME DE-Vol. 35, Rotating Machinery and Vehicle Dynamics, 1991, pp. 191-199

[4] Schmied, M., Pradetto, B.; Drop of Rigid Rotor in Retainer Bearings, *Third Internat. Symp. on Magnetic Bearings, Washington*, July 1992, pp. 145-156

[5] Kirk, R. G., Swanson, E. E., Karavana, F. H., Wang, X.; Rotor Drop Test Stand for AMB Rotating Machinery, *Fourth Internat. Symp. on Magnetic Bearings*, Zurich, 1994

[6] Feeny, B. F.; Stability of Cylindrical and Conical Motions of a Rigid Rotor in Retainer Bearings, *Fourth Internat. Symp. on Magnetic Bearings*, Zurich, Aug. 1994, pp. 229-224

[7] Brite/Euram Project 5463: Modelling of Rotor/Statot Interaction Dynamics (Rostadyn), Bruxelles, Final Report due April 1997

[8] Muszynska, A.; Rotor to stationary element rub-related vibration phenomena in rotating machinery - literature survey, *The Shock and Vibration Digest*, March,1989, pp. 3-11

[9] Isaksson, J. L.; On the Dynamics of a Rotor Interacting with Non-Rotating Parts, *Linkoping University, Thesis No. 426*, Sweden, 1994

[10] Fumagalli, M., Varadi, P., Schweitzer, G.; Impact Dynamics of High Speed Rotors in Retainer Bearings and Measurement Concepts, *Fourth Internat. Symp. on Magnetic Bearings*, Zurich, Aug. 1994, pp. 239-244

[11] Fumagalli , M., Schweitzer, G: Measurements on a Rotor Contacting its Housing. 6th Internat. Conf. on Vibrations in Rotating Machinery, Oxford, Sept. 1996

[12] H.F. Black, Interaction of a Whirling Rotor with a Vibrating Stator across a Clearance Annulus, J. Mech. Eng. Sci., Trans. IFToMM, Vol. 10, 1968, pp.1-12

[13] Lingener, A.; Experimental Investigation of Reverse Whirl of a Flexible Rotor, *Third Internat. Conf. on Rotordynamics*, Lyon, IFToMM, 1990, pp. 13-18